NASA Contractor Report 159125

Multi-Element Airfoil Viscous - Inviscid Interactions

L.W. Gross

MCDONNELL AIRCRAFT COMPANY
MCDONNELL DOUGLAS CORPORATION
St. Louis, Missouri

Contract NAS1-15369
September 1979

National Aeronautics and
Space Administration

Langley Research Center
Hampton, Virginia 23665
AC 804 827-3966

1. Report No.	2. Government Accession No.	3. Recipient's Catalog No.
NASA CR-159125		

4. Title and Subtitle	5. Report Date
MULTI-ELEMENT AIRFOIL VISCOUS-INVISCID INTERACTIONS	6. Performing Organization Code
7. Author(s)	8. Performing Organization Report No.
L. W. Gross	10. Work Unit No.
9. Performing Organization Name and Address McDonnell Aircraft Company McDonnell Douglas Corporation St. Louis, Missouri 63166	11. Contract or Grant No. NAS1-15369
12. Sponsoring Agency Name and Address National Aeronautics and Space Administration Washington, D.C. 20546	13. Type of Report and Period Covered Contractor Report
	14. Army Project No.

15. Supplementary Notes

Langley Technical Monitor: Harry L. Morgan, Jr.
Final Report

16. Abstract

Subsonic viscous-inviscid interactions for multi-element airfoils are predicted by iterating between inviscid and viscous solutions until the performance coefficients converge. Inviscid flow is modelled by using distributed source-vortex singularities on configuration surface panels. Viscous effects are calculated by an existing laminar separation bubble model and a NASA-Lockheed boundary layer-wake method. Numerical formulations and example calculations are presented.

17. Key Words (Suggested by Author(s))	18. Distribution Statement
Multi-Element Airfoils Viscous Flow Viscous-Inviscid Interaction	Unclassified - Unlimited Subject Category 02

19. Security Classif. (of this report)	20. Security Classif. (of this page)	21. No. of Pages	22. Price*
Unclassified	Unclassified	24	

*For sale by the National Technical Information Service, Springfield, Virginia 22161

TABLE OF CONTENTS

LIST OF ILLUSTRATIONS

MULTI-ELEMENT AIRFOIL VISCOUS-INVISCID INTERACTIONS

L. W. Gross
McDonnell Douglas Corporation

SUMMARY

Viscous effects for two-dimensional subsonic multi-element airfoils are calculated by using a combination of the most promising potential flow and viscous flow calculation models. The inviscid flow is modelled by combined source-vortex singularities on configuration surface panels. A prescribed normal velocity distribution is satisfied indirectly by applying an internal perturbation potential boundary condition to the center of each panel. The method is numerically stable, and the prediction accuracy is competitive with more complex curved panel formulations.

Development of the wake and boundary layer and the interaction between them are predicted by a method developed by NASA and Lockheed. Criteria recently established at McDonnell are used to predict the development and bursting of short laminar separation bubbles at the airfoil leading edge. Viscous-inviscid interactions are predicted by iterating between inviscid and viscous solutions until the airfoil performance coefficients converge. The formulation used to model the leading edge flow and sample calculations are presented.

SYMBOLS

A,B,A',B'	Constants
C_D, C_d	Airfoil Section Drag Coefficient
C_L, C_ℓ	Airfoil Section Lift Coefficient
C_m	Airfoil Section Pitching Moment Coefficient (about quarter-chord)
C_n	Airfoil Section Normal Force Coefficient
C_p	Pressure coefficient
c	Airfoil chord
g	One-half of the Leading Edge Radius
H	Boundary Layer Shape Factor
ℓ_1	Distance from Laminar Separation to Transition

ℓ_2	Distance from Transition to Reattachment
M	Mach Number
N	Total Number of Airfoil Elements or Panel Endpoints per Airfoil Element
$\vec{n}$	Unit Vector
R	Airfoil Radius of Curvature
R_c	Reynolds Number Based on Airfoil Chord
R_θ	Reynolds Number Based on Momentum Thickness and Local Velocity
s	Surface Distance
$\vec{V}$	Velocity Vector
x'	Non-Dimensional Distance Along Parabola Axis
x_s'	Distance Along Parabola Axis to Stagnation Point
α	Angle of Attack
γ	Vortex Density
θ	Momentum Thickness
δ^*	Boundary Layer Displacement Thickness
δ	Airfoil Element Deflection Angle
σ	Source Density
ϕ_i	Point Distribution Angle, equation (1)

SUBSCRIPTS

∞	Freestream Conditions
U,L	Upper, Lower
p	Conditions at Peak Velocity
R	Reattachment
s	Conditions at Separation Point
T	Transition

INTRODUCTION

The performance of a multi-element airfoil system is dominated by viscosity. The boundary layer effectively thickens the airfoil and distorts the camber, usually resulting in increased drag and reduced lift. If the boundary layer separates from the airfoil surface, these effects become even stronger.

Because many earlier multi-element airfoil inviscid flow prediction methods were inexact, it was expedient to make empirical corrections for viscosity. However, the availability of efficient and accurate inviscid methods has recently placed renewed emphasis on the analytical prediction of viscous effects through a combined viscous/inviscid analysis approach.

In order to make use of the most promising available methods, the analysis mode of the Multi-Element Airfoil Inviscid Analysis and Design Program (MAAD, reference 1) has been combined with the boundary layer and viscous interaction analysis routines of the NASA-Lockheed program of reference 2. The NASA-Lockheed program predicts boundary layer development, wake development, and confluent wake-boundary layer interaction. Viscous displacement effects are represented by either surface blowing or redefining the effective airfoil geometry. The viscous-inviscid interaction is determined by an iterative recalculation of the inviscid and viscous flows until the overall section performance coefficients do not change appreciably between cycles. The new program is designated the Multi-Element Airfoil Viscous Analysis Program (MAVA).

As a first step toward the inclusion of the capability of calculating separated flows, Herring's criterion for the bursting of short laminar separation bubbles (reference 3) has been incorporated into Program MAVA. This includes calculation of the bubble size, shear layer development across the bubble, and conditions at the point of bubble bursting. Currently the method assumes shear layer reattachment whether or not the bubble bursts. The method can be extended to include calculations across the following types of separation bubbles: (1) trailing edge, (2) leading edge, and (3) long laminar. Such an extension would involve coupling the method of Gross (reference 4) with the mixed analysis-design feature of Program MAAD. The example case shown in figure 1 indicates that this coupling is feasible.

VISCOUS FLOW ANALYSIS METHODS

The development of the viscous flow analysis methods is given in detail in reference 2. This discussion will be restricted to an enumeration of the methods used with an expanded discussion of the changes that were made to include the potential flow method of Program MAAD and the short laminar separation bubble calculation method.

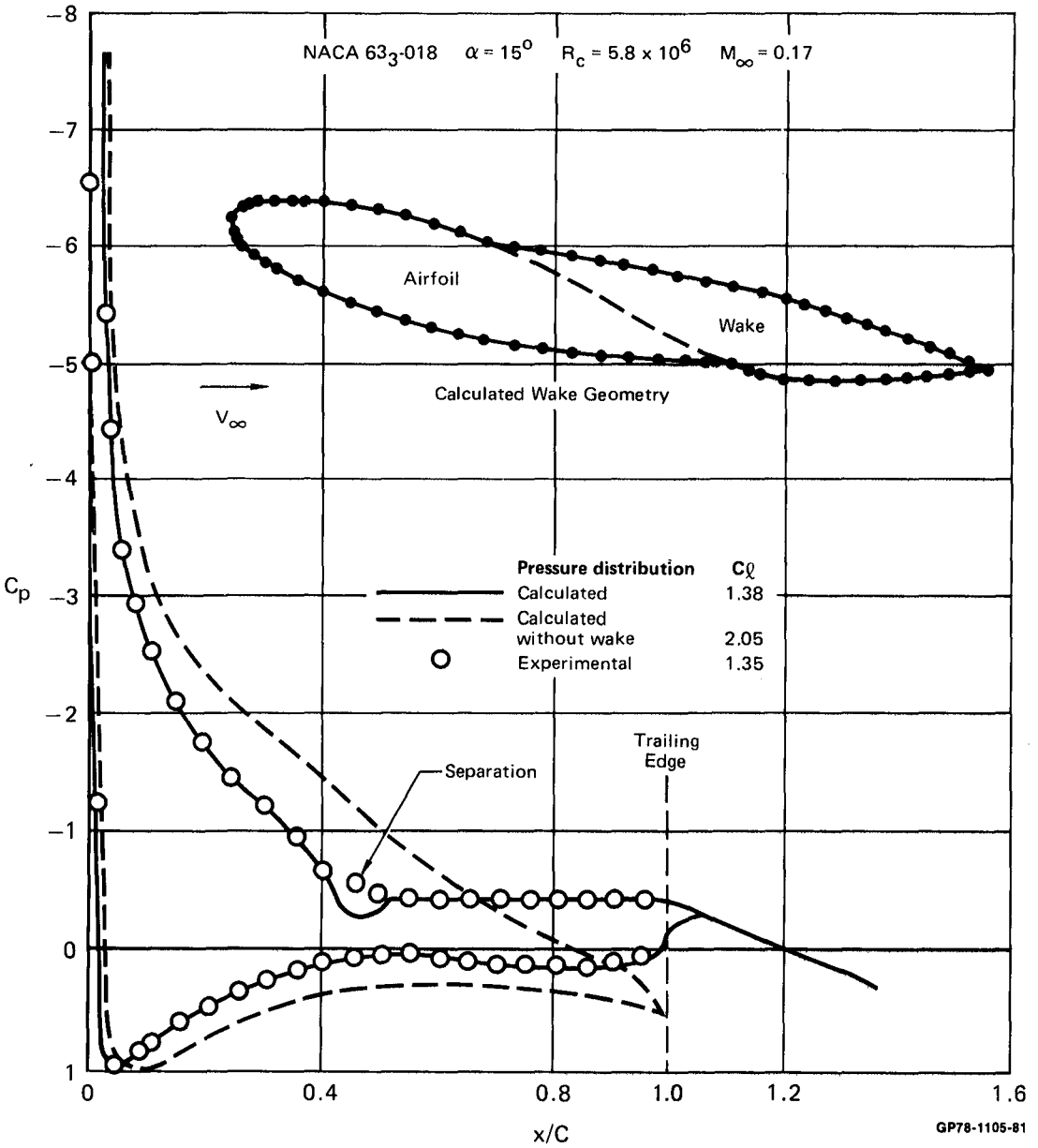

Figure 1. MCAIR Airfoil-Wake Solution Method

In addition to the basic flow characteristics of Mach number and Reynolds number, the user inputs to the program a definition of the shapes of the various airfoil elements, information to align the elements with each other and the free-stream direction, and a specification of the number of panels into which each airfoil element will be divided. Figure 2 shows the basic coordinate system for each airfoil element. The shape of the element is specified by an array of points starting from the leading edge and proceeding to the trailing edge along the upper surface, and then a similar array for the lower surface. The selection of these points is arbitrary. Two auto-

matic panel redistribution methods are included in the program. The first is a cosine method, which distributes the panel end points by means of the formula

$$x_i = \frac{c_j}{2}(1 + \cos\phi_i) \quad \text{where } \phi_i = \frac{i\pi}{N_j},\ i = 1, 2 \ldots N_j \qquad (1)$$

c_j is the chord and N_j is the number of panel end points for the airfoil element in question. The second method closely spaces the points in regions of high curvature. The details of the spacing method are given in reference 2.

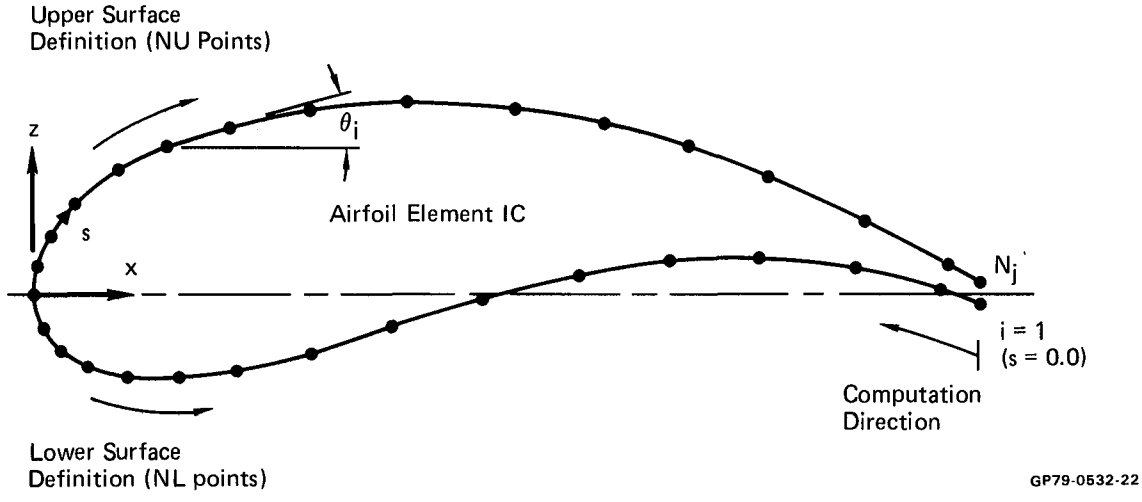

Figure 2. Coordinate System for Multi-Element Airfoil Viscous Analysis Program (MAVA)

A third alternative is to use the panel end points specified by the user. In that case, corresponding panel end points on both upper and lower surfaces should be specified at the same x-locations. The alignment will simplify the division of the airfoil into thickness and camber, to be discussed later.

The program then rearranges the panel end points into the computational array. This array starts at the lower surface trailing edge and proceeds clockwise around the airfoil element surface to the upper surface trailing edge. The computational coordinates are θ vs s, where θ is the local surface angle of the given panel and s is the distance along the surface from the lower surface trailing edge to the panel end point or midpoint.

Each airfoil element is defined in its own coordinate system. The airfoil is then lofted by means of a scale factor for each element and specified pivot points as shown in figure 3. Each airfoil element has between 1 and N-1 pivot points, where N is the total number of elements. The pivot points are used to locate the elements with respect to each other and serve as axes of rotation.

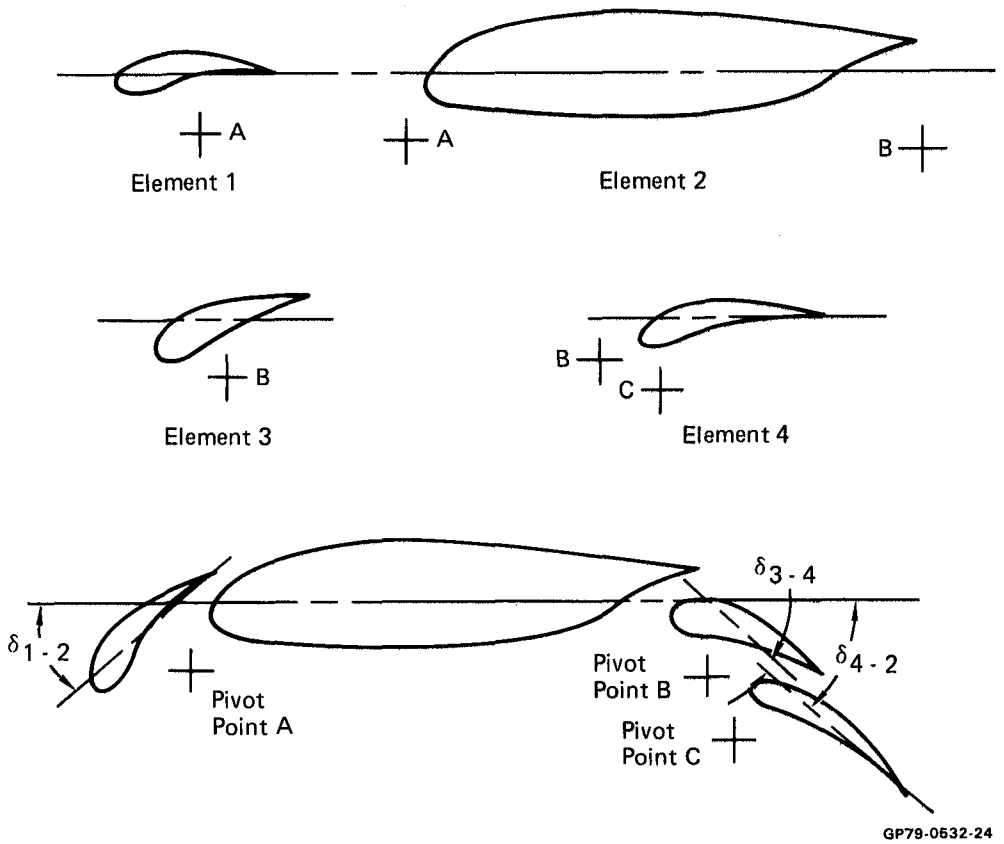

Figure 3. Lofting of a Four Element Airfoil

After the elements have been lofted into a complete airfoil system, the potential flow velocities are calculated by means of the MAAD method. Then the stagnation point is defined as the point where the surface velocity vector changes sign. The airfoil nose is defined as the point where the inwardly directed radius of curvature is a minimum (figure 4). The radius of curvature

$$\frac{1}{R} = \frac{\Delta\theta_i}{\Delta s} \tag{2}$$

is examined only over the forward 75% of the airfoil element chord. This eliminates the possibility that regions of small curvature near the flap cove will be mistaken for the nose. The airfoil camber line is normal to the airfoil surface at the nose. The distance x'_s along the camber line to a point from which a normal is drawn to the stagnation point is determined. The definition of the airfoil camber line and the distance x'_s are required for the study of the short laminar separation bubble, to be described later.

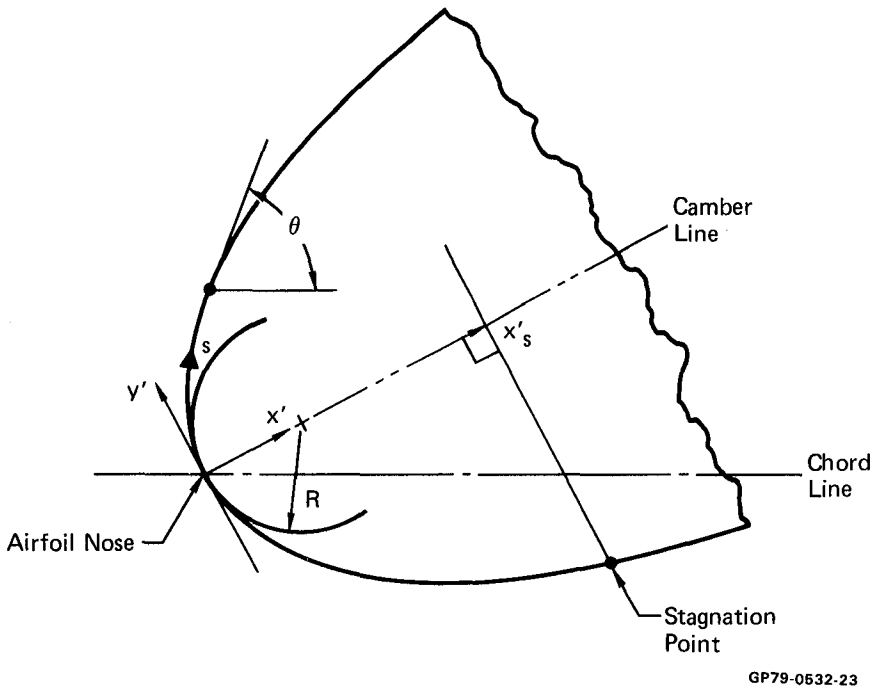

Figure 4. Coordinate System at the Nose of a Cambered Airfoil

The Karman-Tsien compressibility correction is applied to the pressure coefficients computed in the potential flow portion of the airfoil program. Using isentropic flow relations, the local Mach number is computed and input to the boundary layer portion of the program. Then a flat plate boundary layer analysis is performed on each surface of each airfoil element. Starting from the stagnation point, the initial laminar boundary layer development is calculated by the method of Cohen and Reshotko as described in reference 5. After computing the laminar boundary layer characteristics at discrete points, the tests for boundary layer separation or boundary layer instability are performed. Instability is determined by the criterion established by Schlichting and Ulrich, presented in reference 6. If the boundary layer is unstable, a transition check is made based on an empirically derived transition prediction curve. An indication of transition triggers the calculation of initialization quantities for the turbulent boundary layer. If the user inputs a fixed transition location, a check will be made to determine whether or not the specified location has been reached.

If the laminar boundary layer method of Cohen and Reshotko indicates laminar separation, the extent of the laminar separation bubble is calculated. This will be discussed more thoroughly later.

After computing the transition location, or if laminar separation bubble reattachment is indicated, the turbulent boundary layer calculations are made. The Truckenbrodt method described in reference 7 is used.

For multi-element airfoils, there is an interference between the wake of a previous airfoil element and the boundary layer of the following element. This interference region starts at the slot exiting plane between the trailing edge of the forward element and the surface of the aft element. The region can extend to the trailing edge of the aft element, depending upon the pressure distribution. The confluent boundary layer in this region is a result of the mixing between the slot efflux and the wake of the forward element. A model of the confluent boundary layer flow was formulated by Goradia and is presented in reference 8.

The program uses an iterative procedure to obtain the viscous solution. First, a potential-flow solution is computed for the basic airfoil. The boundary layer properties are then computed based on the previous potential flow solution. A modified airfoil is constructed by adding the boundary layer displacement thickness to the original airfoil. The steps are repeated until convergence of the performance coefficients is obtained. The most important step of the procedure lies in the manner by which the modified airfoil is constructed. A proper formulation of this step strongly influences the final answer and the speed of convergence of the iteration. The method developed by Lockheed and described in reference 2 has proven satisfactory. It is retained in the current program.

The Lockheed method is based on the assumption that the boundary layer thickness and camber effects can be treated independently and then superimposed to determine the net effect. The unsymmetrical thickness of the boundary layers on the upper and lower surfaces has a decambering effect near the trailing edge, which causes a reduction in the effective angle of attack and lift coefficient. This camber change is the difference in the magnitude of the upper and lower surface displacement thicknesses. The thickening effect of the boundary layer increases the local surface velocities and lift coefficient. This effect is determined by analyzing two symmetrical airfoils. The first is defined by the thickness distribution of the original airfoil. The second is generated by augmenting the original thickness by the sum of the upper and lower surface displacement thicknesses. The net effect is the difference between the potential flow velocities of the second and first symmetrical airfoils at zero angle of attack.

Figure 5 shows the boundary layer displacement thickness corrections for one of the cases studied. A low Reynolds number case was chosen so that the boundary layer displacement thicknesses would be visible. The addition of the displacement thickness to the symmetrical airfoil produces a thick trailing edge. In actual flow, the wake acts as an afterbody with a rapidly decreasing thickness distribution. As described in reference 2, an analytical expression was developed empirically to represent the afterbody shape.

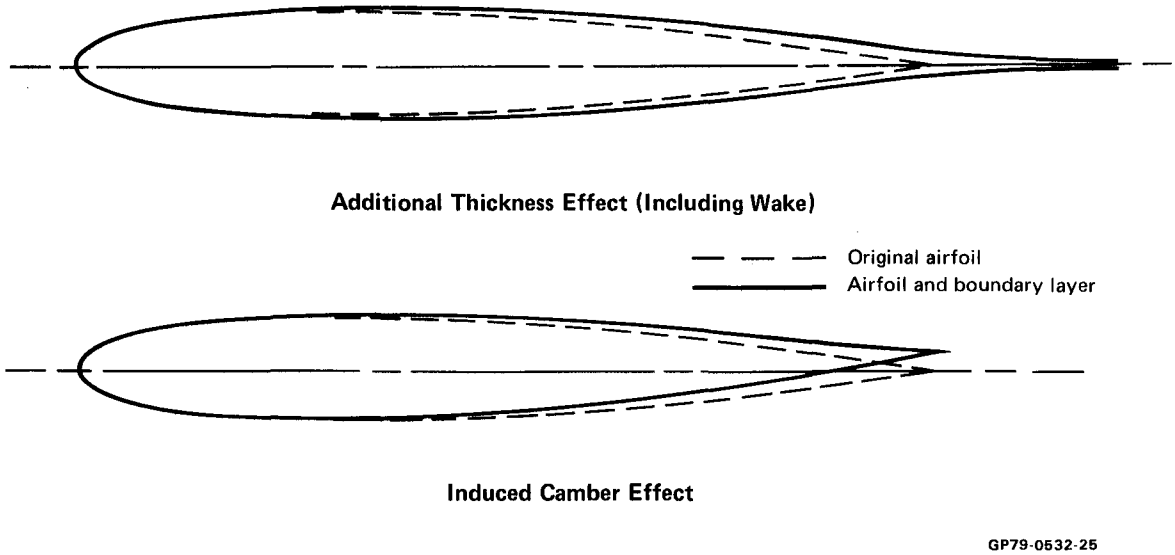

Figure 5. Boundary Layer Displacement Corrections

As described in reference 1, the MAAD potential flow calculation method could be extended to handle airfoils with thick trailing edges. Presently, thick trailing edges are handled approximately. A triangular sliver is removed from the upper and lower surfaces of each airfoil element. The sliver thickness varies from zero at the nose of the element to one-half of the base thickness at the trailing edge. This sliver is then added to the boundary layer displacement thickness on the respective surface and its effect is calculated as described above.

The flow diagram for Program MAVA is presented in figure 6.

SHORT LAMINAR SEPARATION BUBBLES

At reasonably high Reynolds numbers, laminar boundary layer separation is followed quickly by transition to turbulent flow and reattachment to the surface as a turbulent boundary layer. The resulting short separation bubble is typically one or two percent chord long and has only a slight effect on the lift and drag of the airfoil. However, since the rate of growth of a shear layer is greater than that of a boundary layer over the same distance, the presence of the separation bubble has an effect on the subsequent development of the turbulent boundary layer. In addition, bursting, or the failure of the turbulent shear layer to reattach, is the initial event in the formation of a long laminar separation bubble or a leading edge bubble. For these reasons, a model of the short laminar separation bubble and bubble bursting was included in the viscous flow portion of Program MAVA.

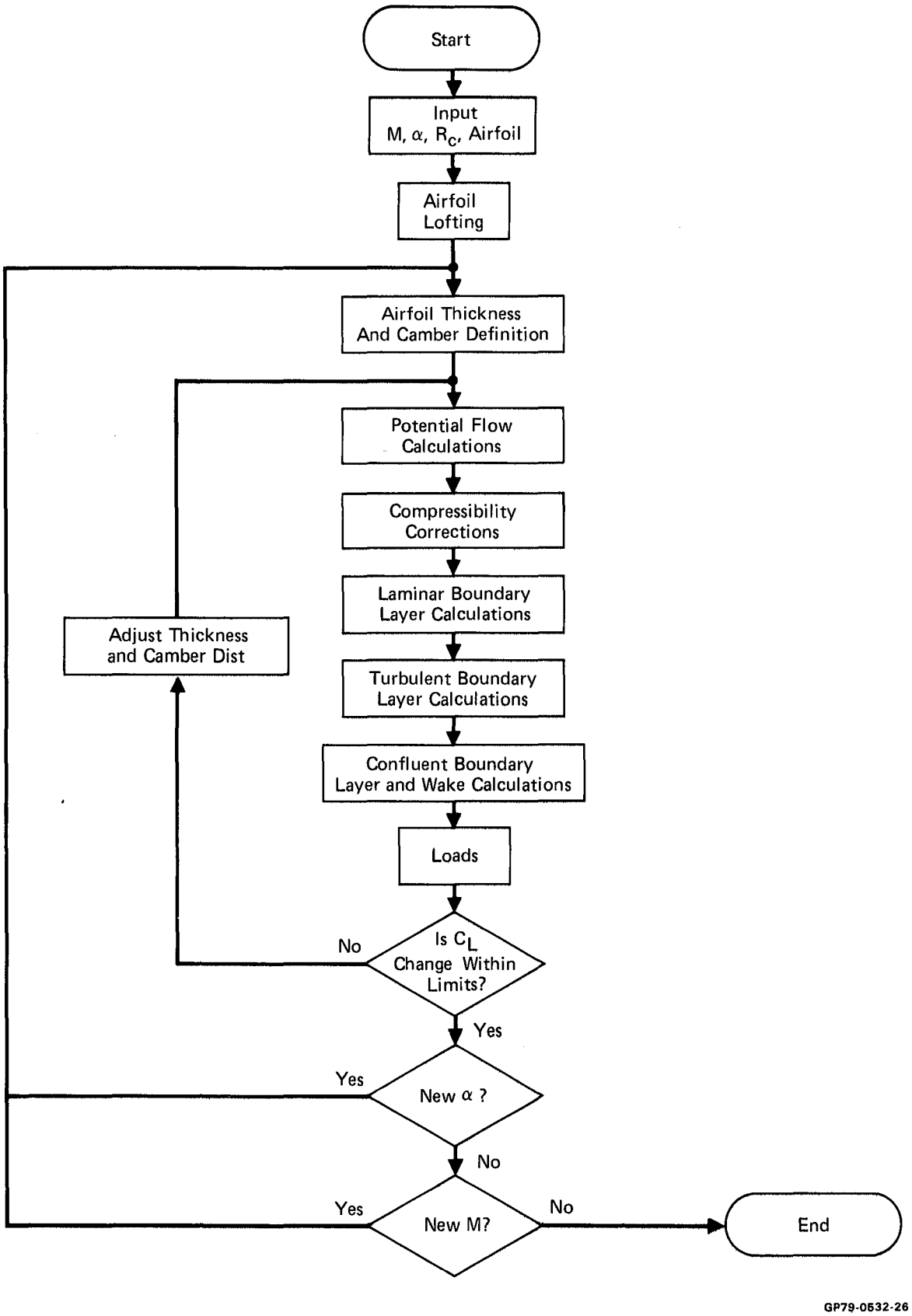

Figure 6. Flow Diagram for MAVA Program

The model of the laminar separation bubble was first proposed by Gaster (reference 9) and developed by Horton (reference 10) and others. Included in reference 9 is a criterion for bubble bursting that can be applied if the separation is not in the immediate vicinity of the leading edge. The case of short laminar separation bubble bursting near the leading edge has been studied extensively by others (references 3, 10, 11 and 12). An empirical correlation developed by Herring (reference 3) is used in Program MAVA.

Gaster's model of the laminar separation bubble is illustrated in figure 7. It is assumed that separation is followed by a constant pressure mixing region controlled by a laminar shear layer. Because a laminar shear layer is unstable, the transition to turbulent flow takes place over a very short distance. The distance to transition is a function of the momentum thickness of the separating boundary layer. Horton determined this distance ℓ_1 empirically as

$$\ell_1 R_{\theta_{sep}} = 4 \times 10^4 \tag{3}$$

This was refined by Vincent de Paul (reference 11) to

$$\ell_1 \theta_{sep} R_{\theta_{sep}} = \left[0.06275 \frac{(1000)}{R_{\theta_{sep}}}\right]^{1.66} \tag{4}$$

Ingen (reference 12) studied the shape of the laminar separation area and concluded that the assumption of a straight separation streamline was more realistic than the assumption of constant pressure. Therefore, he developed a method for calculating the velocity distribution along a straight streamline. By evaluating the disturbance amplification properties of a laminar shear layer, he then developed an improved method for calculating the distance to transition. This involves a quadrature calculation of the amplification factor. An expression useful for rough calculations is

$$\ell_1 R_{\theta_{sep}} = 8.6 \times 10^{-4} \theta_{sep} \tag{5}$$

Once the point of transition is found, the momentum thickness at transition can be determined from the momentum integral equation.

The pressure distribution in the turbulent shear flow region of figure 7 is taken as the Stratford distribution for incipient separation (reference 13). Reattachment is defined as the point where the Stratford pressure distribution intersects the undisturbed potential flow pressure distribution. Inci-

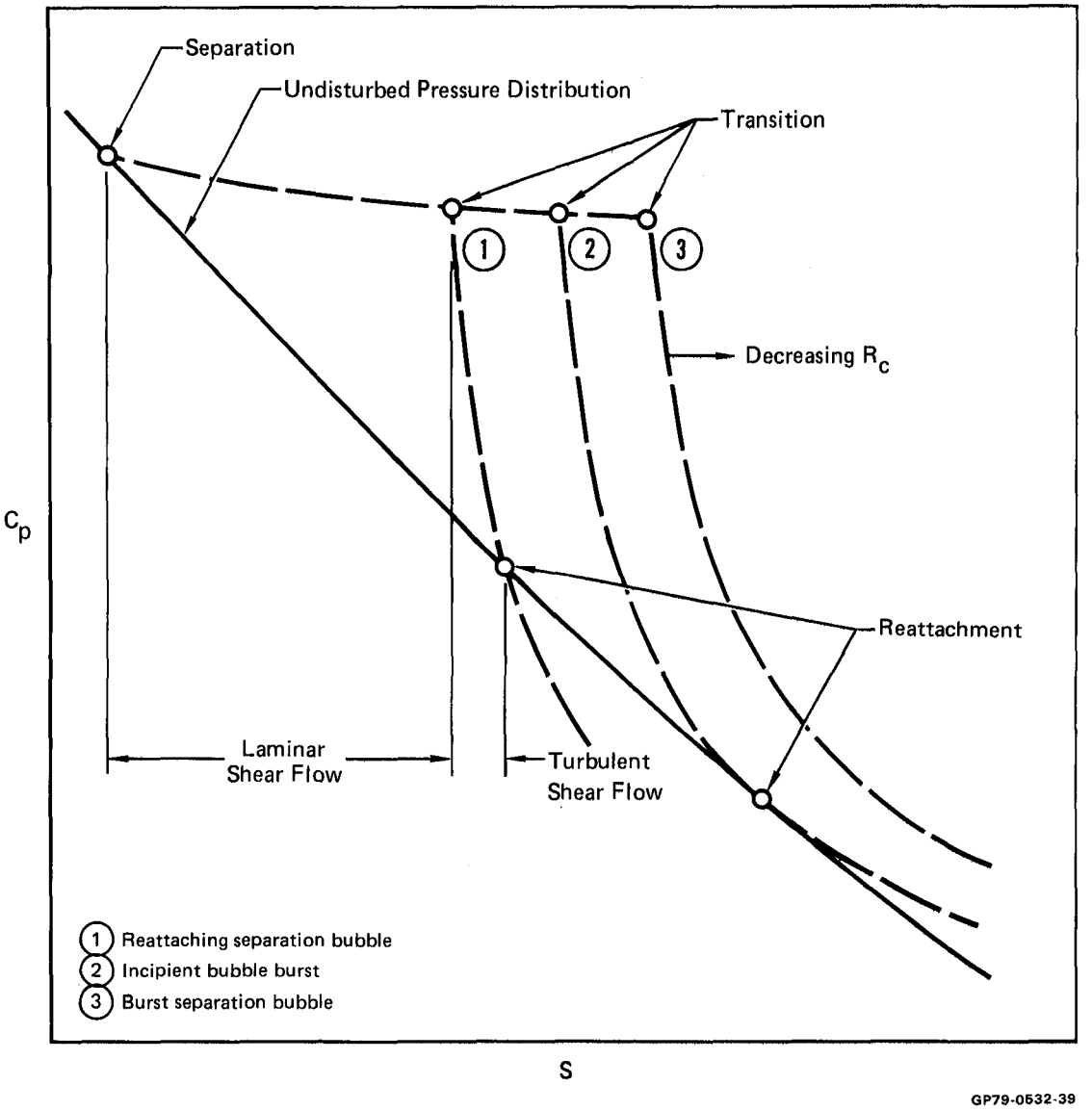

Figure 7. Schematic Diagram of a Short Laminar Separation Bubble Pressure Distribution

pient bubble bursting occurs if the Stratford pressure distribution is tangent to the undisturbed pressure distribution. If the two pressure distributions do not intersect, the bubble is considered to have burst.

After the short laminar separation bubble has burst, the shear layer follows a streamline of the flow. Since the pressure in the resultant large bubble is lower than ambient pressure, this streamline curves back toward the airfoil. Under certain conditions of airfoil thickness/chord ratio or camber distribution, the shear layer will intersect the airfoil surface. In this case, the resultant flow is designated a long laminar separation bubble. In other cases, an upper surface shear layer can intersect a lower surface shear layer downstream from the airfoil

trailing edge. This characterizes a leading edge separation bubble. For both cases, the provision has not yet been made to calculate the flow around these bubbles. Therefore, the program determines the point of closest approach of the Stratford pressure distribution to the undisturbed pressure distribution and, after printing an appropriate comment, sets this point as the point of shear layer reattachment.

After the point of reattachment is established, the boundary layer parameters are calculated by assuming a linear pressure distribution between transition and reattachment. The momentum integral equation then can be solved in closed form.

$$\theta_R^2 = \frac{1}{\bar{V}_R^6}\left[\theta_T^2 + \frac{0.075\, \ell_2\, (\bar{V}_R^6 - 1)}{\frac{\bar{V}_T}{V_\infty} R_C\, (\bar{V}_R - 1)}\right] \tag{6}$$

where $\bar{V}_R = V_R/V_T$, $\ell_2 = s_R - s_T$ and the subscripts R and T refer to reattachment and transition respectively.

If laminar separation occurs very near the leading edge, Herring's method is applied (reference 3). Herring concludes that local pressure gradients are typically too large to be adequately defined by conventional interpolation methods. However, if an approximate analytical expression could be found for the pressure distribution, the definition of the pressure gradient would be straightforward. Therefore, Herring approximates the nose of an airfoil by a parabola. The parabola selected is the one which matches the radius of curvature at the airfoil nose. The axis of the parabola coincides with the camber line at the nose, where the nose is defined as the point of minimum radius of curvature. The velocity distribution on an infinite parabola at an angle of attack α is

$$\frac{V}{V_\infty} = \frac{A \cos\alpha \pm B \sin\alpha \sqrt{\frac{1 - x'}{x'}}}{\frac{ds}{dx'}} \tag{7}$$

where the + sign corresponds to the upper surface and the - sign the lower. The distance x' is a non-dimensional distance along the axis of the parabola, starting from its nose. The slope of the surface of a parabola can be written as

$$\frac{ds}{dx'} = \sqrt{\frac{g + x'}{x'}} \tag{8}$$

where

$$g = \frac{l}{2} \text{ (leading edge radius)}$$

therefore

$$\frac{V}{V_\infty} = \frac{A\sqrt{x'}\cos\alpha \pm B\sqrt{1 - x'}\sin\alpha}{\sqrt{g + x'}} \tag{9}$$

$$\simeq \frac{A\sqrt{x'}\cos\alpha \pm B\sin\alpha}{\sqrt{g + x'}}$$

$$\simeq \frac{A'\sqrt{x'} \pm B'}{\sqrt{g + x'}}$$

for a given angle of attack.

At the leading edge ($x' = 0$)

$$\frac{V}{V_\infty} = \frac{B'}{\sqrt{g}} \tag{10}$$

At the stagnation point ($V = 0$)

$$\frac{x'_s}{g} = \left(\frac{B'}{A'\sqrt{g}}\right)^2 \tag{11}$$

The peak velocity is

$$V_p = A'\sqrt{1 + \frac{x'_s}{g}} \tag{12}$$

at

$$\frac{x'_p}{g} = \frac{1}{x'_s/g} \tag{13}$$

The constant g is one-half of the radius of curvature at the nose, and the constants A and B are determined from the velocity distribution calculated by the MAAD method. B corresponds to

the velocity at the nose (determined by a second-order interpolation, if necessary) and A is evaluated at the stagnation point (figure 4).

For a parabola, the quantities A and B are constants and are equal to unity. When this expression is applied to an airfoil, however, A and B are nonunity and are functions of x'. Nevertheless, a family of velocity distributions are provided that fit those of a wide variety of airfoils. The boundary layer development for this family of velocity distributions was calculated by the method of Thwaites (reference 14), and the point of separation was determined by the method of Stratford (reference 15). In this manner, a consistent set of boundary layer solutions was provided that fits most airfoils of interest. By applying the solutions to a body of available data on laminar separation bubble burst, a correlation curve

$$\left[\frac{V_s}{V_\infty}\left(\frac{dV/V_\infty}{ds/c}\right)_{sep}\frac{g}{c}\right]_{burst} = -\left[0.4838 \times 10^{-12} R_c \frac{V_s}{V_\infty}\frac{g}{c}\right]^{1/7}$$

was established with only a narrow scatter band. The correlation curve relates a Reynolds number based on velocity at the separation point and the leading edge radius with a separation pressure gradient parameter scaled by the leading edge radius.

This leading edge approximation is used only for a single element airfoil or the leading element of a multi-element airfoil. Because subsequent elements of a multi-element airfoil operate in the superimposed flow field of preceding elements, the approximation of flow around a parabola does not apply.

The flow diagram for the laminar boundary layer calculations is shown as figure 8. The Herring correlation for short laminar separation bubble bursting is applied immediately. The first calculation is for the position and magnitude of the nose radius of curvature, performed in subroutine NOSER. This calculation, plus the position of the stagnation point and the calculated velocities near the nose, are input to subroutine SHØRTB. This routine calculates the existence of laminar separation near the nose. If separation occurs and the positions of the separation point and stagnation point are within the limits of applicability of the Herring correlation, a test for bubble bursting is made. Currently, a prediction of bubble bursting causes only a warning statement to be printed.

If separation predicted by subroutine SHORTB is within the proper limits, subroutine VINGEN is called. This subroutine requires the boundary layer parameters at separation and the velocity distribution. It then calculates the conditions at transition and reattachment. If subroutine VINGEN fails to find a solution, instantaneous transition at the separation point is assumed.

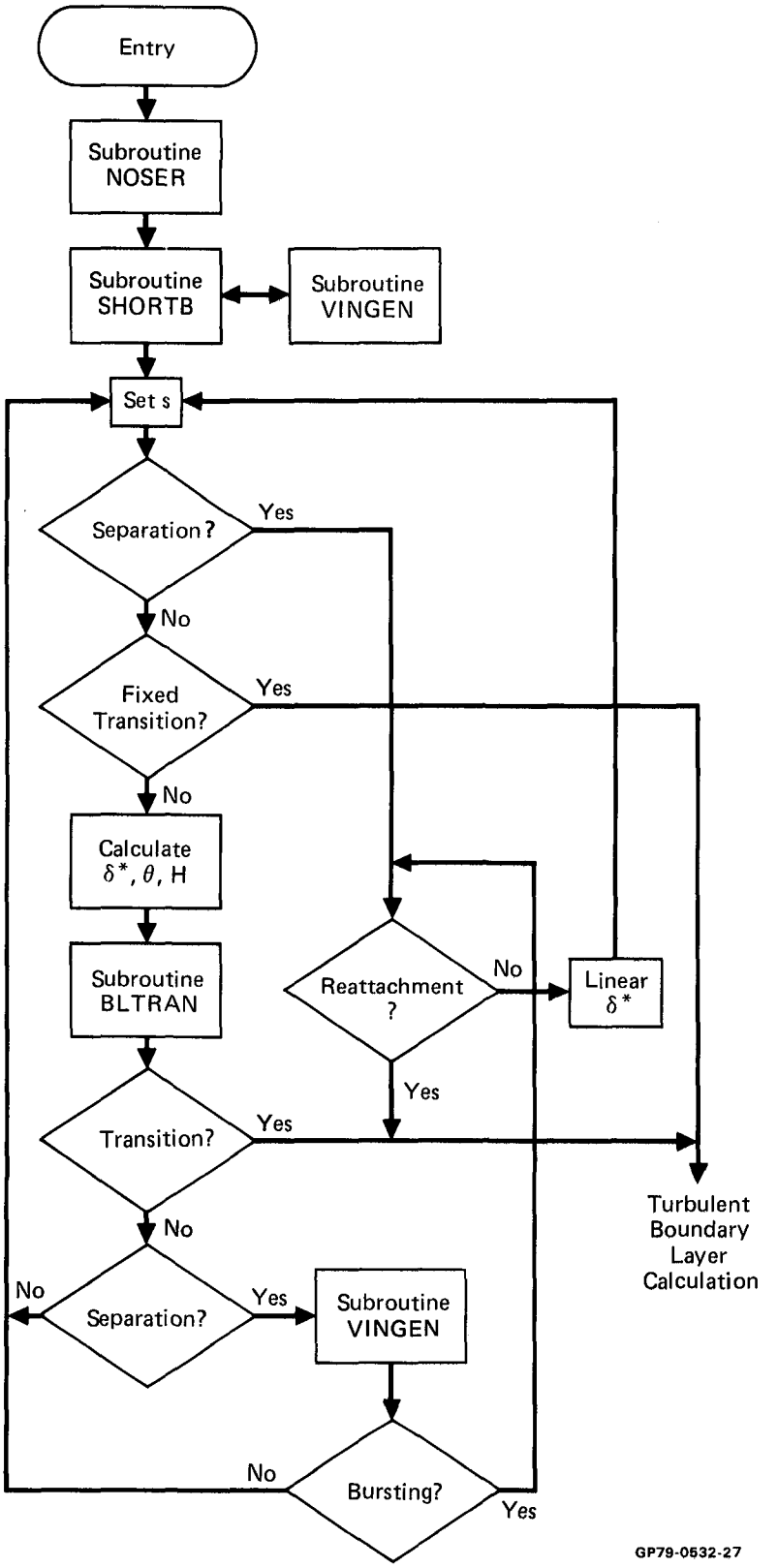

Figure 8. Flow Diagram for Laminar Boundary Layer Calculations Including Leading Edge Separation Bubble

Prior to each incremental calculation of the laminar boundary layer development, a test is made to determine whether fixed transition or separation has occurred. If transition is indicated, an exit is made to the turbulent boundary layer calculations. If separation is predicted, it is assumed that the boundary layer displacement thickness varies linearly between its values at separation and reattachment. At reattachment, the exit is made to the turbulent boundary layer calculations.

EXAMPLE CALCULATIONS

The purpose of the example calculations was two-fold. First it was desired to compute the viscous lift loss for attached flow predicted by the Multi-Element Airfoil Viscous Analysis program (MAVA) with both experiment and an alternative calculation method. Secondly, it was desired to demonstrate the ability of the short laminar separation bubble prediction method incorporated in the program to determine leading edge stall of an airfoil. For these reasons, an analysis was made of the NACA 0012 airfoil. This airfoil was selected because there is a large body of experimental data available (references 16 through 19). Also, reference 19 shows a comparison of the experimental stall data with predictions of short laminar bubble bursting by other methods.

Program MAVA also has been checked out for a four-element high lift airfoil. Although the comparison with experimental force and pressure data is reasonable, the viscous effects are so small that the comparison is dominated by the accuracy of the potential flow calculations. Therefore, that multi-element solution is not considered appropriate for presentation here. Clearly, further evaluation is required for multi-element configurations.

Calculations of the viscous flow on the NACA 0012 airfoil were made at chord Reynolds numbers $R_c \times 10^{-6} = 0.5$, 1.0, 3.0 and 6.0 in order to cover the full range for which experimental data is available. The stalling data and bubble burst calculations of reference 19 indicated that stalling occurred by laminar separation bubble bursting at Reynolds numbers less than $R_c = 3.0 \times 10^6$ and by trailing edge separation at higher Reynolds numbers.

The ability of the MAVA program to predict the viscous lift loss for single element airfoils is demonstrated by the results of figure 9. This figure shows the variation of the normal force coefficient divided by $\sin \alpha \cos \alpha$ as a function of the angle of attack α. $C_N/\sin \alpha \cos \alpha$ is the exact form of the lift curve slope and is theoretically constant for incompressible flow. Changes of the lift curve slope are induced primarily by the viscous effects and are the most sensitive indicator of these effects. It can be seen that the inviscid calculations by the method of Melnik (reference 20) vary with

angle of attack only by an amount ascribable to the effects of compressibility. Melnik adapted the transonic conformal transformation method due to Garabedian and Korn to include the effects of viscosity. Therefore, his method should have an inviscid accuracy comparable to other conformal transformation methods. The MAVA inviscid calculations, on the other hand, show an increase of the lift curve slope with angle of attack. This level of increase (2% at $\alpha = 20°$) is attributed to the use of the Karman-Tsien compressibility correction.

The experimental data shows an approximately 12% loss of lift curve slope due to viscosity. This loss is relatively constant over the angle of attack range from $\alpha = 0°$ to $\alpha = 14°$ at which point the airfoil stalls. At $\alpha = 14°$, there is a 2% uncertainty band which is probably due to the differing wind tunnel conditions of the different tests. The MAVA program calculated a 15.5% viscous lift loss at the low angles of attack which decreased at the higher angles of attack. Beyond $\alpha = 14°$, the point of turbulent boundary layer separation moved substantially ahead of the trailing edge. The MAVA program cannot make reasonable predictions at higher angles of attack since it does not contain a model for the trailing edge separation bubble. However, the calculations were continued in order to determine the behaviour of the short laminar separation bubble at the airfoil leading edge and are included for completeness.

Comparison runs were made with the viscous version of the Melnik program at $R_c = 6 \times 10^6$. In addition to calculating the boundary layer development, Melnik calculates the flow in the wake and connects the two viscous flow regions with a triple-deck, large interaction viscous flow model at the airfoil trailing edge. The method also includes the effect of the pressure jump across the wake due to wake curvature. The viscous effects are then coupled with the potential flow calculation method using blowing boundary conditions. This method predicted a 7% reduction of the lift curve slope at the low angles of attack and an 11% reduction at $\alpha = 14°$.

Figure 10 illustrates the method used to determine the existence of short laminar separation bubble bursting. Shown are the bubble burst correlation curve from reference 3 and the values calculated by the MAVA program for the angles of attack and Reynolds numbers studied. It can be seen that at a constant chord Reynolds number, changes of angle of attack cause only a small change of the nose radius Reynolds number but a large change of the velocity gradient parameter. Thus, at low values of chord Reynolds number, the velocity gradient curve for the given airfoil crosses the correlation curve at low angles of attack. As chord Reynolds number is increased, the conditions for bubble burst require a higher velocity gradient, corresponding to a higher angle of attack. In addition, the increase of the velocity at laminar boundary layer separation causes the constant Reynolds number curve to approach the correlation curve asymptotically. This also increases the angle of attack at which the curves will intersect.

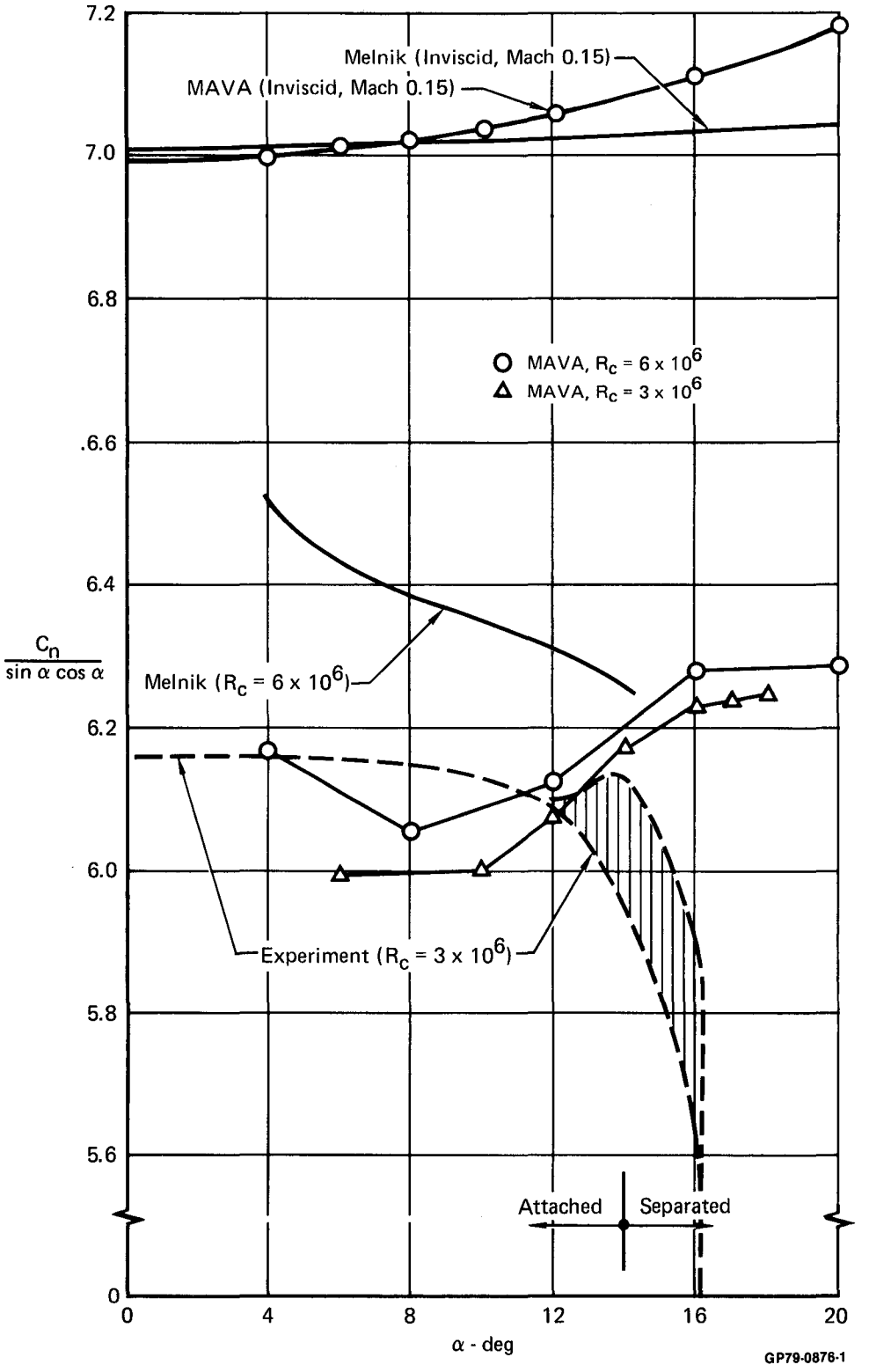

Figure 9. Normal Force Predictions for NACA 0012 Airfoil

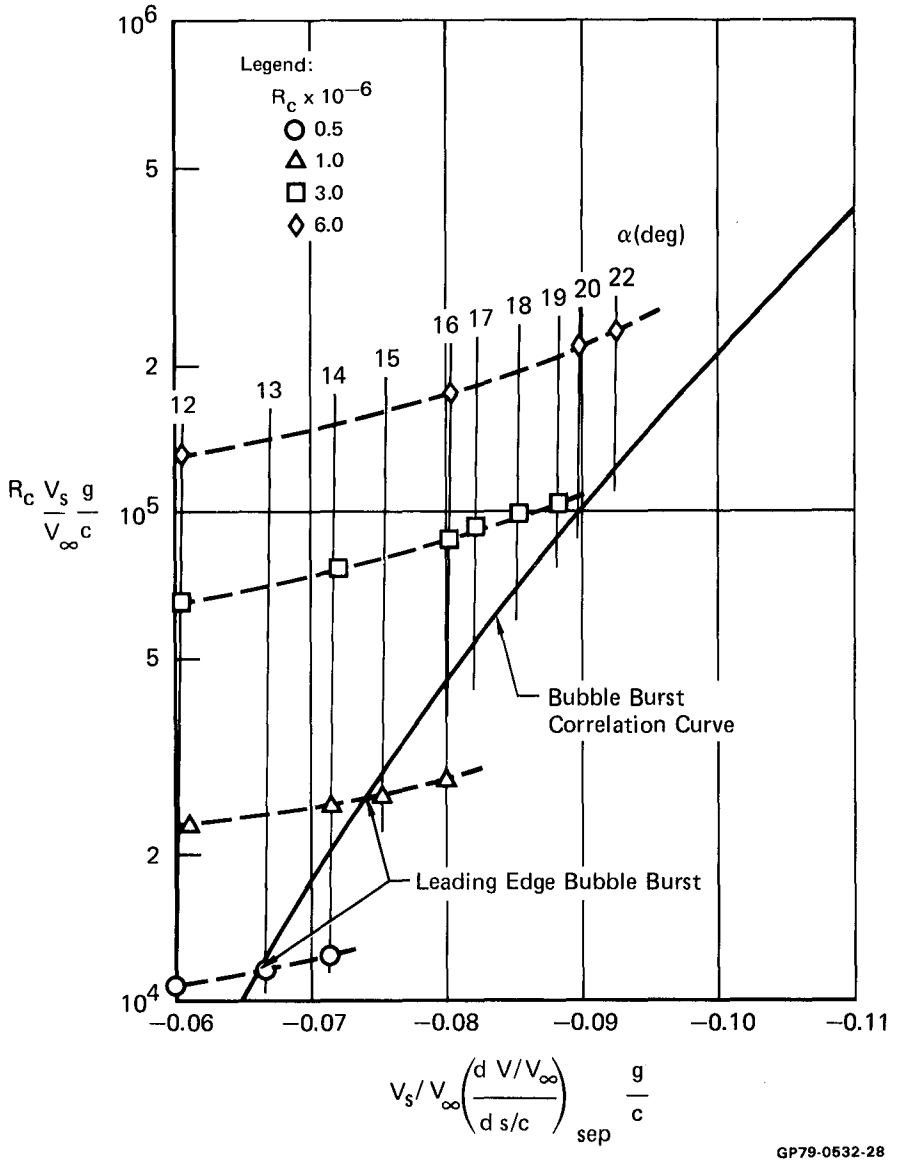

Figure 10. Leading Edge Separation Bubble Burst Prediction
NACA 0012 Airfoil
Mach 0.15

The increase of angle of attack necessary to increase the velocity gradients for laminar boundary layer separation referred to above also increase the velocity gradients over the rest of the airfoil. This, in turn, leads to earlier turbulent boundary layer separation. As turbulent separation moves ahead of the trailing edge, the existence of a trailing edge separation bubble reduces the circulation around the airfoil which, in turn, reduces the velocity gradients near the nose of the airfoil. However, the effect of the trailing edge separation bubble is not yet included in the MAVA program. Therefore, the program could be predicting short laminar separation bubble bursting whereas, in fact, the airfoil is stalling due to the effects of

trailing edge separation. This is illustrated in figure 11. Turbulent separation is defined at the point where the turbulent boundary layer shape factor $H = \delta^*/\theta = 2.0$. The chordwise points at which the MAVA program predicted turbulent separation in this manner are shown for the four chord Reynolds numbers studied. Also shown are the angles of attack at which short laminar separation bubble bursting was predicted from figure 10. It can be seen that there is a slow forward movement of turbulent separation with increasing α up to a certain angle of attack. Beyond that angle of attack, the forward movement is very rapid. It is difficult to judge from figure 11 just where maximum lift occurs, but it is reasonable that stall will be associated with this rapid forward movement. Therefore, for the purposes of this study, trailing edge stall is considered to occur at the angle of attack where the forward projection of the trace of slow forward movement intersects the backward projection of the trace of the rapid forward movement of separation. These points are indicated in figure 11 as the points of trailing edge stall.

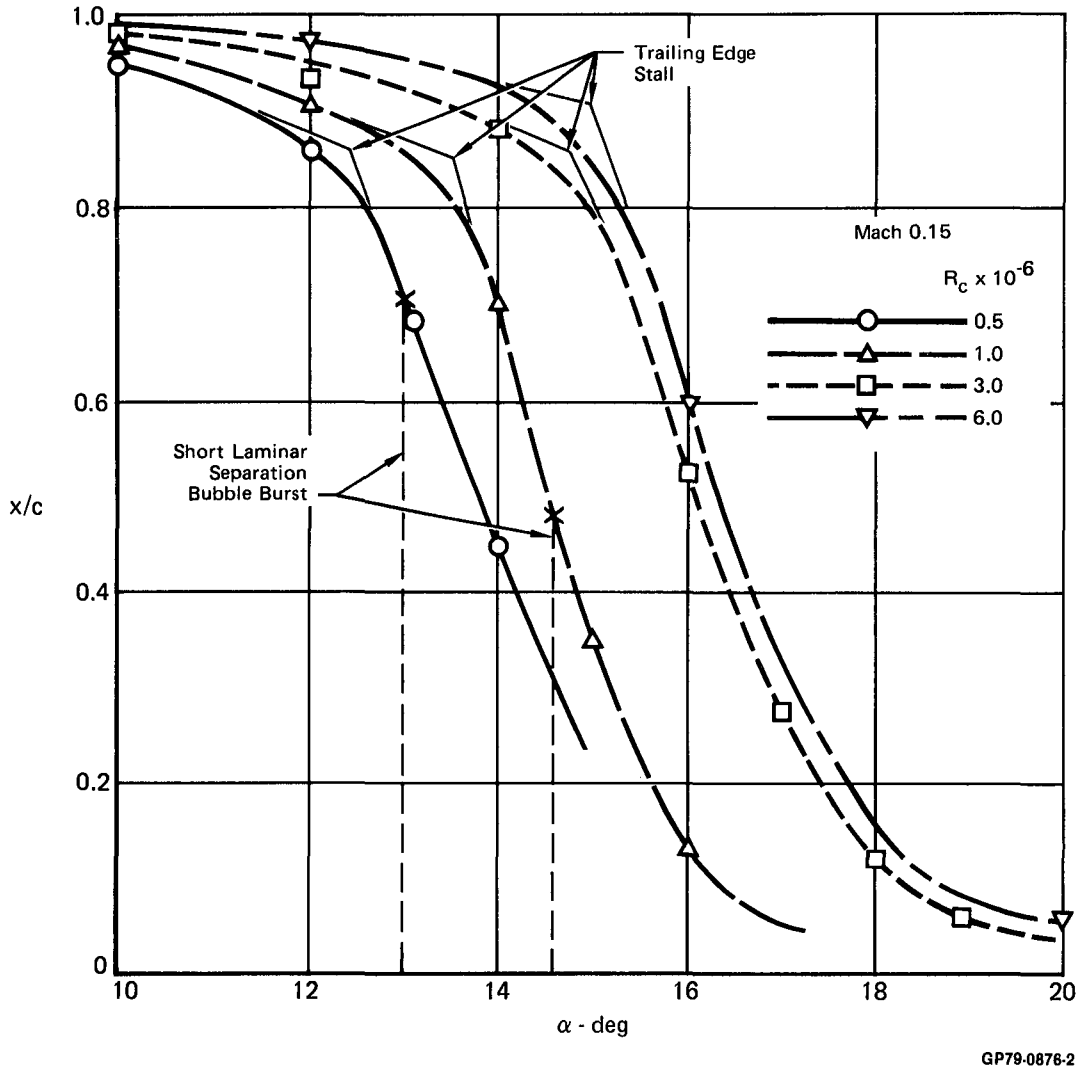

Figure 11. Predicted Upper Surface Separation Location for NACA 0012 Airfoil

The angles of attack for short laminar separation bubble bursting and trailing edge stall as defined above are shown in figure 12. Also shown are the range of experimental stall data and the predictions of other laminar separation bubble bursting methods taken from reference 19. It can be seen that the trend of the laminar separation bubble burst predictions by the MAVA program follow the experimental trends better than do the other methods. The calculations also suggest that the 0012 airfoil does not stall due to laminar separation bubble bursting even at the lowest chord Reynolds number studied. Since the point of rapid forward movement of turbulent separation is predicted to occur at a lower angle of attack than is laminar separation bubble bursting, stall should be due to turbulent separation. The agreement with experiment for this type of stall is good, considering that the flow model for trailing edge stall is incomplete.

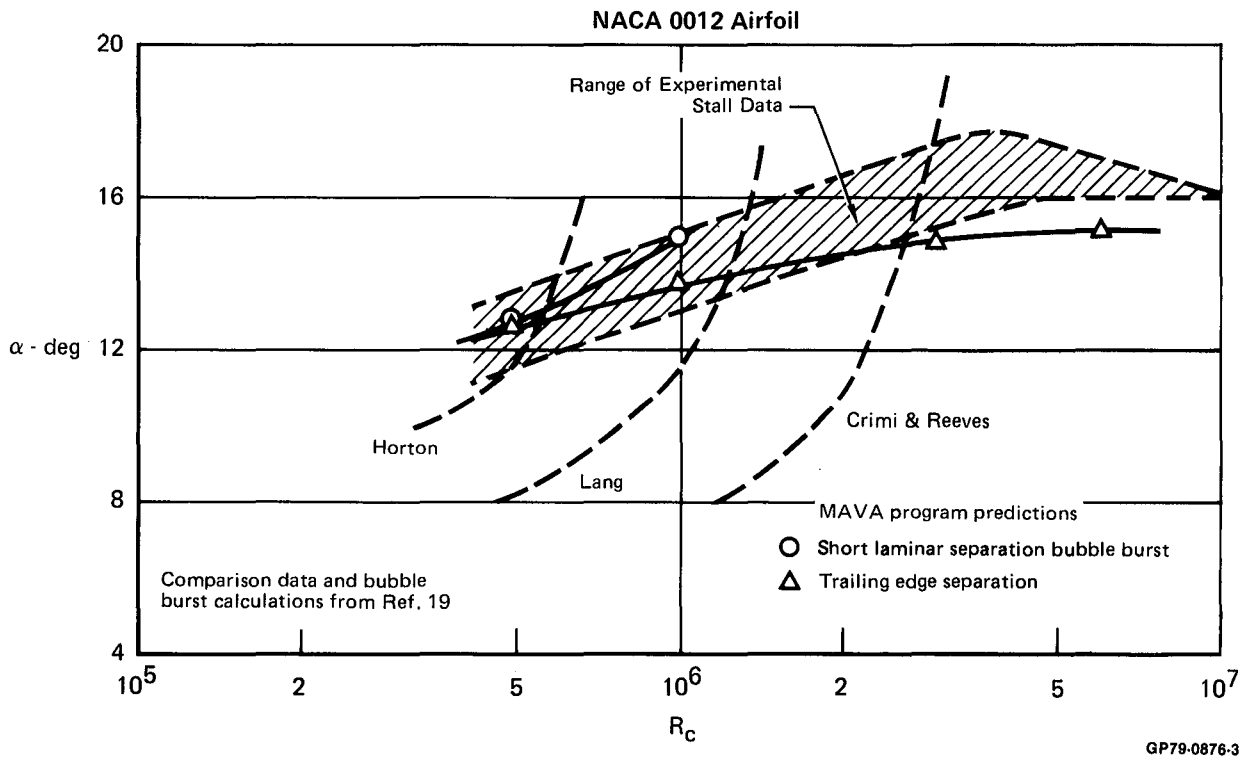

Figure 12. Low Speed Stall Predictions by MAVA Program

CONCLUSIONS

Incorporation of the Multi-element Airfoil Analysis and Design (MAAD) program and the Herring correlation for short laminar separation bubble bursting into the NASA-Lockheed program has resulted in the Multi-element Airfoil Viscous Analysis Program. This program can serve as the first step in the development of a viscous analysis program that is capable of predicting the flow around an airfoil with large areas of separated flow present. The resultant Multi-element Airfoil Viscous Analysis Program (MAVA Program) was used to calculate the viscous lift loss and stalling characteristics of a NACA 0012 airfoil over a range of chord Reynolds numbers. Agreement with experiment was good for the predictions of viscous lift loss at higher Reynolds numbers. The prediction of stalling characteristics also was good over the full range of chord Reynolds numbers for which experimental data was available; although the predicted type of stall was not as stated in the reference from which the experimental data was taken.

REFERENCES

1. Bristow, D.R.: Development of Panel Methods for Subsonic Analysis and Design. NASA CR (to be published), September 1979.

2. Morgan, H.L., Jr.: A Computer Program for the Analysis of Multi-Element Airfoils in Two-Dimensional, Subsonic, Viscous Flow. NASA SP-347, Aerodynamic Analysis Requiring Advanced Computers Conference, Langley Research Center, March 1975.

3. Ely, W.L. and Herring, R.H.: Laminar Leading Edge Stall Prediction for Thin Airfoils. AIAA Paper 78-1222, July 1978.

4. Gross, L.W.: The Prediction of Two-Dimensional Airfoil Stall Progression. AIAA Paper 78-155, January 1978.

5. Cohen, C.B. and Reshotko, E.: The Compressible Laminar Boundary Layer with Heat Transfer and Arbitrary Pressure Gradient. NACA Rep. 1294, 1956. (Supersedes NACA TN 3326).

6. Schlichting, H. (J. Kestin, transl.): Boundary-Layer Theory". Sixth ed., McGraw-Hill Book Co., Inc., 1968.

7. Truckenbrodt, E.: A Method of Quadrature for Calculation of the Laminar and Turbulent Boundary Layer in Case of Plane and Rotationally Symmetrical Flow. NACA TM 1379, 1955.

8. Goradia, S.H.: Confluent Boundary Layer Flow Development With Arbitrary Pressure Distribution. Ph.D. Thesis, Georgia Inst. of Technology, 1971.

9. Gaster, N.: The Structure and Behavior of Separation Bubbles. British ARC R&M 3595, March 1967.

10. Horton, H.P.: A Semi-Empirical Theory for the Growth and Bursting of Laminar Separation Bubbles. British ARC Report CP-1073, 1969.

11. Vincent de Paul, M.: Prevision du Decrochage d'un Profile d'Aile en Ecoulement Incompressible. AGARD CP-102, Flow Separation, November 1972.

12. Ingen, J.L. van: On the Calculation of Laminar Separation Bubbles in Two-Dimensional Incompressible Flow. AGARD CP-168, Flow Separation, 1975.

13. Stratford, B.S.: The Prediction of Separation of the Turbulent Boundary Layer. Journal of Fluid Mechanics, Volume 5, 1959, pp. 1-16.

14. Thwaites, B.: Approximate Calculation of the Laminar Boundary Layer. Aero Quarterly, 1949, pt. I, pp. 245-280.

15. Stratford, B.S.: Flow in the Laminar Boundary Layer Near Separation. British ARC R&M 3002, 1957.

16. Jacobs, E.N. and Sherman, A.: Airfoil Section Characteristics as Affected by Variations of the Reynolds Number. NASA Report 586, September 1937.

17. Yip, L.P. and Shubert, G.L.: Pressure Distributions on a 1-by-3 Meter Semispan Wing at Sweep Angles from 0° to 40° in Subsonic Flow. NASA TN D-8307, December 1976.

18. Gregory, N., Quincey, V.G., O'Reilly, C.L. and Hall, D.J.: Progress Report on Observations of Three-Dimensional Flow Patterns Obtained During Stall Development on Aerofoils, and on the Problem of Measuring Two-Dimensional Characteristics. NPL Aero Report 1309, January 1970.

19. McCroskey, W.J. and Phillipe, J.J.: Unsteady Viscous Flow on Oscillating Airfoils. AIAA Paper 74-182, January 1974.

20. Melnik, R.E.: Wake Curvature and Trailing Edge Interaction Effects in Viscous Flow Over Airfoils. NASA CP-2045, Advanced Technology Airfoil Research, March 1978.